An Innovative Approach to Dynamics Modeling and Simulation of the Molten Salt Rector Experiment

Conference Paper · September 2014

CITATIONS
2

READS
406

4 authors, including:

Lelio Luzzi
Politecnico di Milano
173 PUBLICATIONS **1,282** CITATIONS
SEE PROFILE

Antonio Cammi
Politecnico di Milano
169 PUBLICATIONS **1,267** CITATIONS
SEE PROFILE

Carlo Fiorina
École Polytechnique Fédérale de Lausanne
56 PUBLICATIONS **368** CITATIONS
SEE PROFILE

PHYSOR 2014 – The Role of Reactor Physics Toward a Sustainable Future
The Westin Miyako, Kyoto, Japan, September 28 – October 3, 2014, on CD-ROM (2014)

AN INNOVATIVE APPROACH TO DYNAMICS MODELING AND SIMULATION OF THE MOLTEN SALT RECTOR EXPERIMENT

M. Zanetti, L. Luzzi, A. Cammi[1]
Department of Energy - CeSNEF (Centro Studi Nucleari Enrico Fermi)
Politecnico di Milano, Milano, Italy
matteo.zanetti@polimi.it
lelio.luzzi@polimi.it
antonio.cammi@polimi.it

C. Fiorina[2]
FAST Group - Laboratory for Reactor Physics and Systems Behavior
Paul Scherrer Institute, Villigen PSI, Switzerland
carlo.fiorina@psi.ch

ABSTRACT

The Molten Salt Reactor Experiment (MSRE) was a circulating fuel thermal reactor built and operated in the sixties. As the only Molten Salt Reactor (MSR) testing facility for which extensive experimental data are available, it can be considered as a reference for the development of modeling approaches for the studies related to the Gen-IV MSR. In this work, a geometric multi-scale approach has been adopted for the simulation of the MSRE plant. The data and the experimental results relative to the U-233 fuelled reactor are considered. The neutronic parameters have been determined using the Monte Carlo code Serpent. The reactor core is divided into three radial regions, each one described by a 3D channel in which Navier-Stokes and energy conservation equations plus delayed neutron precursors (DNP) balance equations are solved. Determination of the generated power is obtained employing a point kinetics like equation, fed with importance weighted values of temperatures and DNP concentrations. The remaining part of the plant, that includes the primary and secondary cooling circuits, is modeled by means of zero-dimensional components. The results attained with such modeling approach are compared with experimental data both in time and frequency domain, showing good agreement. The adopted approach, thanks to the punctual, coupled solution of the governing equations in the core, gives better insights into the thermal behavior of the graphite and its effects on MSR dynamics than commonly used correlation-based solvers.

Key Words: **Molten Salt Reactor, Multi-Physics, Geometric Multi-Scale, MSRE.**

1. INTRODUCTION

The Molten Salt Reactor Experiment (MSRE) was built in the 1964 at the Oak Ridge National Laboratory (ORNL, USA) and operated for about 13000 hrs in the frame of a Project for the development of liquid fuelled reactors. The MSRE was an 8 MW_{th} thermal reactor in which the liquid fuel flowed into graphite channels. On the basis of the experience on the MSRE, the 2400 MW_{th} Molten Salt Breeder Reactor was designed [1], but the Project was stopped for lack of funding. Nowadays, the interest in the MSRE can be found in two main reasons: 1) it can be used as a test case for MSR modeling approaches; and 2) it represents a technology basis for some re-

[1] http://www.nuclearenergy.polimi.it/
[2] http://fast.web.psi.ch/

cent projects like the FUJI reactor (2008) [2] and the TMSR (2011) [3] from Chinese Academy of Science which still relies on a graphite moderator. Scope of this work is to illustrate MSRE modeling obtained by the adoption of a geometric multi-scale approach based on a "Multiphysics" (MP) solution for the graphite channels and a 0D description of out-of-core plant components. The MSRE is chosen as the test case for the peculiarities of MSR modeling, also allowing for comparison with experimental data. The adoption of this approach allows a less demanding computational power while retaining the gains from the pure MP one. The paper is divided in 4 sections: introduction; modeling approach; obtained results; and conclusions.

2. MSRE PLANT MODELLING

The MSRE plant (for the main features, see [4]) has been subdivided into two main regions: the core and the out-of-core parts. The core, approximated to a cylinder, has been divided into three radial zones of equal volume, selected in order to have the intermediate one to be also representative of average reactor conditions (Table 1). Each zone has been simulated by a 3D equivalent channel, modeling heat transfer, salt flow and Delayed Neutron Precursors (DNP) transport with Partial Differential Equations (PDE) and solving them with COMSOL® Multiphysics [5]. The temperature, the mass flow and the DNP outlets are then passed to the out-of-core components of the plant. The reactor power is governed by a point-kinetics like power equation, fed with the *neutronic importance* weighted average value of fuel and graphite temperature in the core and the DNP concentration. The out-of-core part includes the two reactor plena, the piping, the primary Heat Exchanger (HE) and the secondary HE, all modeled with a 0D approach. The plena allow for temperature and precursors mixing, and take into account the generation of a fraction of the reactor power. The plena temperature is also taken into account for the reactivity feedback determination. The heat exchangers have been modeled through a mean logarithmic temperature description.
The modeling is further detailed in the following subsections, and is summarized in Figure 1.

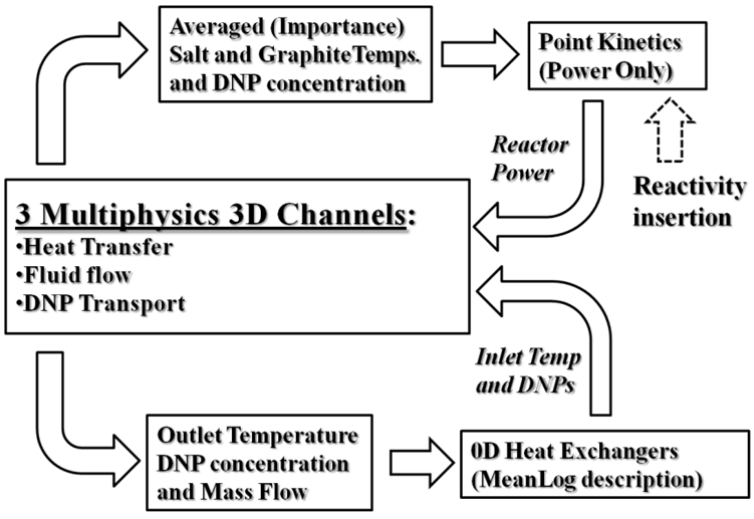

Figure 1. Conceptual scheme of the overall plant modeling.

Table 1. Core radial zone division. The reported Power Fraction coefficient is the amount of the total Core power generated into the zone.

Cylinder height 1.65 m	**Zone 1**	**Zone 2**	**Zone 3**
Radial limits, cm	[7;41]	[0;7]∪[41;57.2]	[57.2;70]
Power fraction, %	49	36	15

2.1. Determination of Neutronic Parameters

Due to the peculiar modeling approach, a calculation of the main feedback coefficients is necessary, possibly taking into account the reactor geometry with a good approximation. An extensive analysis of the MSRE feedback coefficients was performed in the frame of the MOST Project [6]. However, for our analysis, the salt feedback coefficient has to be subdivided for the core salt and plena. Therefore, we performed a new computation of the reactivity coefficients. The Monte Carlo code Serpent/PSG2[7] has been selected for the computation.
The salt composition was taken from [8], the density was determined from [9] and its formulation with respect to the temperature is reported in section 2.2.

The MSRE was designed to be operated with 3 control rods, each one constituted by 36 annular elements (about 3.8 cm long with an inner radius of 1.067 cm and an outer radius of about 1.37 cm) strung on a flexible stainless steel hose. The control elements have been considered in the composition 30% Al_2O_3 - 70% Gd_2O_3, with a density of 5.78 g cm^{-1} [10]. The three control rods have been set to a position of criticality at 900 K. The reactor was inserted into a cylindrical thermal shield, in which the reactor chamber had the radius of 1.19 m and the height of 3 m. The gap between the inner and the outer wall of the shield was 40 cm width, filled with water-cooled steel spheres, so that the composition of the shield was roughly of 50% water and 50% carbon steel. Moreover, the internal wall was covered by a thermal insulator of 15.2 cm width. For its composition we referred to [11], in which it was modeled as expanded vermiculite.

The temperature reactivity coefficients have been computed for the temperature interval of [900 K; 1200 K], taking into account the consequent salt density variation and graphite expansion. Moreover, the void reactivity coefficient has been computed for the two temperatures defined above, considering a homogeneous distributions of the voids.
The feedback coefficients have been computed as:

$$\alpha_x = -\frac{1}{k_{eff}}\frac{\Delta k_{eff}}{\Delta x} \tag{1}$$

where x is the perturbed variable and k_{eff} is the effective multiplication factor.
The results are reported in Table 2 and 3. The geometry and an example of the solution obtained with Serpent are reported in Figures 2 and 3.

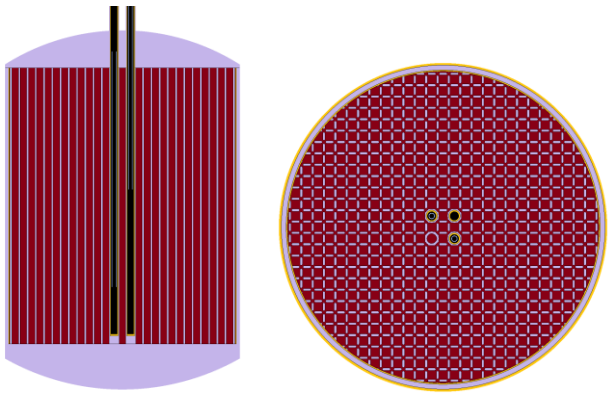

Figure 2. MSRE geometry adopted for Serpent simulation. On the left, a vertical cross section, about 5 cm from the mid-plane, is shown; on the right, the horizontal cross section at the mid-plane is represented. The thermal shield is not reported.

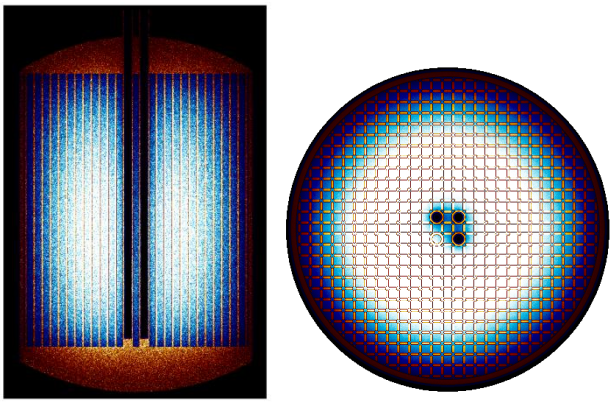

Figure 3. Serpent simulation of MSRE. Colors from red to yellow represent relative fission power, while the interval from blue to white represents the relative thermal flux (below 0.625 eV). The cross sections are taken as in Figure 2. The thermal shield is not represented.

The results are in reasonable agreement with the ones from MOST Project and ORNL computations, as reviewed in [6]. Differences are related to the fact that the latter ones did not take into account the presence of the control rods in the core and the thermal shield. In fact, the introduction of these two components was found to be important to attain a good estimate of the feedbacks in the plena, due to the change in the flux shape, the absorptions in the upper plenum and the reflection effects. The graphite temperature coefficient is lower in our configuration than average MOST results and the overall salt coefficient is higher. The void coefficients are of the same order of magnitude as those predicted by ORNL [12].

Table 2. Temperature reactivity coefficients α_T and their standard deviation, computed with Serpent, JEFF 3.1 cross section library. The salt coefficient has also been computed for different zones: the core, the downcomer, and the Upper and Lower Plenum (U.P. and L.P.). The reference k_{eff} has been taken equal to 1.00415 (0.011%), at 900 K; thermal induced expansion in the graphite and salt density variations are taken into account. The results are compared with the average values from MOST Project (average of deterministic based values and their standard deviation, JEFF 3.1 library) and ORNL computations [6].

α_T, *pcm K*$^{-1}$	Total	Graphite	Salt	Core	Downc.	L.P.	U.P.
	-17.64	-4.5	-13.64	-11.97	-0.35	-1.01	-0.84
St.Dev, %	0.41	1.6	0.56	0.6	19.6	6.7	8.2
ORNL	-16.8	-5.8	-	-11	-	-	-
MOST, avg.	-15.25	-5.2	-	-10.05	-	-	-
MOST, St.Dev.	1.55	0.6	-	0.964	-	-	-

Table 3. Void reactivity coefficient α_V and its standard deviation, computed with Serpent, JEFF 3.1 cross section library. The coefficient is computed with respect to the percent presence of void in the salt.

	900 K	1200 K
α_V, *pcm / %*	-530	-578
St.Dev, %	3.75	4.15

2.2 Core Model

As mentioned, the core has been divided into three zones, each one represented by an equivalent 3D channel. Each channel is built and solved using the finite elements software COMSOL® Multiphysics. The adoption of such software was driven by the option to link it to MATLAB® Simulink [13] for the 0D modeling. The Simulink software leads the simulation, selecting the time-step according to the ODE15s solver settings [13]. When the information on the channel state variables is required, the COMSOL transient solver is started for a limited time (a multiple of the Simulink time-step), for which the inner time-step is determined by the time dependent BDF solver in COMSOL [5]. The geometric modeling of each channel makes use of symmetries and the effective geometry is equivalent to one fourth of a channel, as shown in Figure 4. Each channel is split in four equal parts.

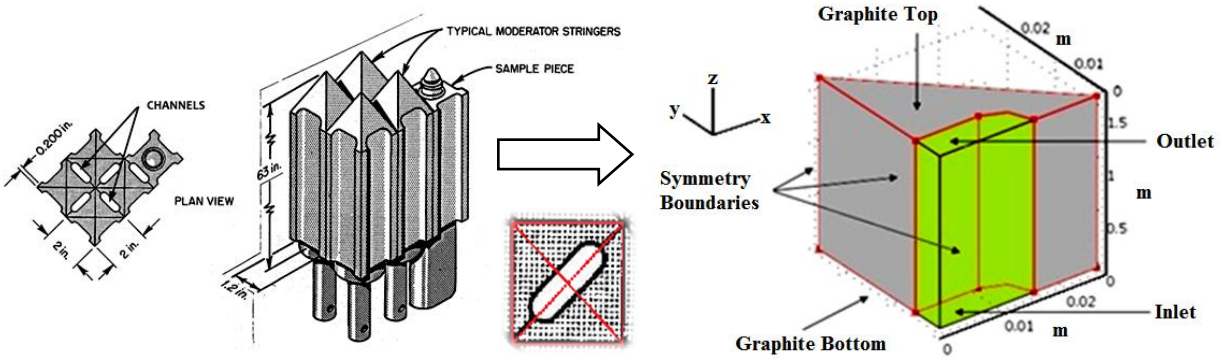

Figure 4. Fuel channel geometry [4] and modeling with general boundary conditions.

On the proposed geometry, three coupled physical phenomena are considered: fluid flow (eq. (2,3), since the flow regime in the channels is laminar no turbulence model has to be considered); heat transfer, modeled with the energy conservation equation (eq. (4)); DNP advection and diffusion, with the source term from fissions (eq. (5)). The equations are written in non-conservative form, as it is common in Finite Element based discretization approach:

$$\frac{\partial \delta}{\partial t} + \nabla \cdot (\delta \mathbf{u}) = 0 \tag{2}$$

$$\delta \frac{\partial \mathbf{u}}{\partial t} + \delta (\mathbf{u} \cdot \nabla)\mathbf{u} = \nabla \cdot \left(-p\mathbf{I} + \mu \left((\nabla \mathbf{u}) + (\nabla \mathbf{u})^{T} \right) - \frac{2}{3} \mu (\nabla \cdot \mathbf{u}) \mathbf{I} \right) - \mathbf{g}\, \delta \tag{3}$$

$$\delta\, c_p \frac{\partial T}{\partial t} + \delta\, c_p \mathbf{u} \cdot \nabla T = \nabla \cdot (\mathbf{k} \nabla T) + Q \tag{4}$$

$$\frac{\partial c_i}{\partial t} + \mathbf{u} \cdot \nabla c_i = \nabla \cdot (D \nabla c_i) + \beta_i \frac{Q}{q_0} - \lambda_i c_i \tag{5}$$

where $\boldsymbol{u}$ is the velocity field, p is the pressure field, T is the temperature field and c_i is the DNP concentration for the i^{th} group. Equations (2,3,5) are not solved in the solid graphite domain. The parameter q_0 is a conversion constant such that Q/q_0 can replace the fission rate in equation (5). The vector $\mathbf{g}$ is the gravity field, directed along the z axis. The meaning of the other symbols and their values are summarized in Table 4. The boundary conditions for equations (2-5) are described in Figure 4. On the split planes, symmetry boundary conditions are used. At the inlet, the velocity is imposed with a "laminar inlet" weak formulation [15], while uniform temperature and precursor

concentration are imposed. The values are determined by the circuit closure (see section 2.3, for the out-of-core models), and are weighted with the measured inlet velocity field on the three zones [16]. At the outlet, a pressure of 2 bar is imposed with the conditions of no viscous stress (i.e., the right-hand term in equation (3) is only dependent from the gravity field), while "outflow conditions" (i.e., zero normal gradient) are considered for the precursors and the energy equations. The top and the bottom of graphite are considered to be thermally insulated. The reactor is simulated with a fixed flux, assuming the power shape computed by ORNL, which takes into account DNP motion [14]. The power source term Q(**r**,t) in equations (4) and (5) has been modeled as:

$$Q(\mathbf{r},t) = \theta_m \, Ch_{Pw} \, n(t) \sin\left(\frac{z + 11.07}{197.35}\right) \tag{6}$$

in which *z* is expressed in cm, the time dependent coefficient is an input determined by point kinetics (equation (7)), the constant Ch_{Pw} is defined for each zone in Table 1 as the power fraction, and the parameter θ_m takes into account the material in which the power is generated. According to ORNL, 6.3% of the core power is promptly generated into the graphite [4].
The reactor power is obtained with a point-kinetics like approach:

$$\frac{dn(t)}{dt} = n(t)\left(\frac{\rho_{IN}}{\Lambda} - \frac{\beta_M}{\Lambda} + \alpha_f \frac{(< T_f(\mathbf{x},t) > - < T_f(\mathbf{x},0) >)}{\Lambda} + \alpha_g \frac{\left(< T_g(\mathbf{x},t) > - < T_g(\mathbf{x},0) >\right)}{\Lambda} + \frac{\rho_{EXT}}{\Lambda}\right) + \sum \lambda_i < c_i(\mathbf{x},t) > \tag{7}$$

where *n* is the power, ρ_{IN} is the inserted reactivity, ρ_{EXT} is the reactivity contribution from the plena and the downcomer, computed with respect to the variation of their mean temperature (0D components). The coefficient β_M is the effective DNP fraction - computed with DNP motion (See 3.1) -, α is the feedback coefficient, Λ is the mean generation time, λ_i is the decay constant for the precursor group *i*, the subscripts *s* and *g* represent the salt and the graphite, respectively. The values for the constants are reported in section 3.
An opportune weighting has to be performed when building the point reactor model from a full dimensional one [18]. We adopted the following average definition:

Table 4. Main parameters adopted for solution of equations (2-5).

	Symbol	Value	Units	Ref.
Density, salt	δ	2.575 - 5.13 10^{-4} T(°C)	g cm^{-3}	[9]
Density, graphite	δ	1874	g cm^{-3}	[17]
Thermal conductivity, salt	K	1.44	W $m^{-1}K^{-1}$	[9]
Thermal conductivity*, graphite	k	53	W $m^{-1}K^{-1}$	[17]
Heat capacity, salt	c_p	1983	J kg^{-1} K^{-1}	[9]
Heat capacity, graphite	c_p	1772	J kg^{-1} K^{-1}	[17]
Dynamic viscosity, salt	M	7.44	mPa s	[9]
Precursor diffusion coefficient	D	5 10^{-9}	m^2 s^{-1}	†

*In the present work, the graphite is considered isotropic.
†The precursor diffusivity is unknown. However, the order of magnitude is known in a general sense and it is here adopted. In fact, the contribution of diffusion is far lower than the advection one and it could be neglected in laminar flow into a channel with a reasonably high flow velocity, as in our case. The diffusive term in Eq.(5) is here included for the sake of generality, especially considering its importance in the case of fast-spectrum MSRs.

$$< f(\mathbf{x},\mathrm{t}) > = \frac{\int \varphi^*(\mathbf{x})\, f(\mathbf{x},\mathrm{t})\, \mathrm{s}(\mathbf{x},\mathrm{t})\, \mathrm{dV}}{\int \varphi^*(\mathbf{x})\, \mathrm{s}(\mathbf{x},\mathrm{t})\, \mathrm{dV}} \tag{8}$$

for the temperature and

$$< f(\mathbf{x},\mathrm{t}) > = \frac{\int f(\mathbf{x},\mathrm{t})\ \mathrm{s}(\mathbf{x},\mathrm{t})\, \mathrm{dV}}{\Lambda \int \varphi^*(\mathbf{x})\, \mathrm{s}(\mathbf{x},\mathrm{t})\, \mathrm{dV}} \tag{9}$$

for the precursor term. In formulas 8 and 9, the term $\varphi^*(\mathbf{x})$ is the adjoint flux for the stationary problem, or the importance function, and $\mathrm{s}(\mathbf{x},\mathrm{t})$ is the flux shape function, which allows to express the neutron flux as $\varphi(\mathbf{x},\mathrm{t}) = \mathrm{n}(\mathrm{t})\mathrm{s}(\mathbf{x},\mathrm{t})$. The shape function is considered time-invariant and equal to the static flux. The same assumptions are adopted for the importance function, namely: $\varphi^*(\mathbf{x}) = \mathrm{s}(\mathbf{x},\mathrm{t}) = \varphi(\mathbf{x},0)$. Such approach is generally considered acceptable for small perturbations.

2.3 Out-of-Core Models

The components in the out-of-core part of the plant are the reactor plena with the downcomer and the two heat exchangers. The plena and the downcomer are modeled with conservation equations:

$$\sum\nolimits_{\mathrm{j}} \dot{\mathrm{m}}_{\mathrm{j,in}}(\mathrm{t}) = \dot{\mathrm{m}}_{\mathrm{out}}(\mathrm{t}) \tag{10}$$

$$\frac{\mathrm{d}}{\mathrm{dt}}\, \mathrm{M}\, \mathrm{T}_{\mathrm{out}}(\mathrm{t})\, \mathrm{cp}_{\mathrm{salt}} = \left(\sum\nolimits_{\mathrm{j}} \dot{\mathrm{m}}_{\mathrm{j,in}}\ \mathrm{T}_{\mathrm{j,in}}\, \mathrm{cp}_{\mathrm{salt}}\right) - \dot{\mathrm{m}}_{\mathrm{out}}\, \mathrm{T}_{\mathrm{out}}(\mathrm{t})\, \mathrm{cp}_{\mathrm{salt}} + \mathrm{Q_f}\, \mathrm{n}(\mathrm{t}) \tag{11}$$

$$\mathrm{c}_{\mathrm{i,out}}(\mathrm{t}) = \left(\sum\nolimits_{\mathrm{j}} \dot{\mathrm{m}}_{\mathrm{j,in}}\ \mathrm{c}_{\mathrm{j,i,in}}(\mathrm{t}) \Big/ \sum\nolimits_{\mathrm{j}} \dot{\mathrm{m}}_{\mathrm{j,in}}\right) + \mathrm{e}^{-\lambda_{\mathrm{i}}\mathrm{t}} \int_0^{\mathrm{t}} \mathrm{e}^{\lambda_{\mathrm{i}}\tau}\, \mathrm{Q_f}\, \frac{\beta_{\mathrm{i}}}{\Lambda}\big(\mathrm{n}(\tau) - \mathrm{n}(0)\big)\, \mathrm{d}\tau \tag{12}$$

where $\dot{m}$ is the mass flow (the subscript *j* takes in a value between *1* and *3* in the upper plenum and is *1* otherwise), *M* is the mass of salt present in the component, estimated from geometric properties [4], Q_f is a factor that takes into account the power generated in the salt with respect to the total reactor power, as computed by Serpent. The values are reported in Table 5. For the purpose of the energy transport, all the piping is simply modeled with pure time delays, as reported in Table 6. The DNP transport in the circuit is modeled analogously, taking into account the decay during the transit time. The intermediary heat exchanger (Salt-Salt) is a U-tube type, in which the secondary (coolant) salt flows around the tubes. The secondary heat exchanger (Salt-Air) is a cross-flow type in which the air-cooled salt flows into the tubes. Both the heat exchangers are modeled with a mean logarithmic temperature approach. Denoting with the *cd* and *cl* subscripts the hot fluid and the coolant, respectively, the salt temperatures are determined from the following equations:

$$\frac{\mathrm{dT_{cd,out}}}{\mathrm{dt}} = -\frac{2}{\mathrm{M_{cd}cp_{cd}}}\left(\dot{\mathrm{m}}_{\mathrm{cd}}\mathrm{cp}_{\mathrm{cd}}\left(\mathrm{T}_{\mathrm{cd,out}} - \mathrm{T}_{\mathrm{cd,in}}\right) + G\ \mathrm{A\ h}\ \Delta\mathrm{T}_{\mathrm{lm}}\right) - \frac{\mathrm{dT_{cd,in}}}{\mathrm{dt}} \tag{13}$$

$$\frac{\mathrm{dT_{cl,out}}}{\mathrm{dt}} = -\frac{2}{\mathrm{M_{cl}cp_{cl}}}\left(\dot{\mathrm{m}}_{\mathrm{cl}}\mathrm{cp}_{\mathrm{cl}}\left(\mathrm{T}_{\mathrm{cl,out}} - \mathrm{T}_{\mathrm{cl,in}}\right) - G\ \mathrm{A\ h}\ \Delta\mathrm{T}_{\mathrm{lm}}\right) - \frac{\mathrm{dT_{cl,in}}}{\mathrm{dt}} \tag{14}$$

$$\Delta\mathrm{T}_{\mathrm{lm}} = \left(\mathrm{T}_{\mathrm{cd,in}} - \mathrm{T}_{\mathrm{cl,in}}\right) - \left(\mathrm{T}_{\mathrm{cd,out}} - \mathrm{T}_{\mathrm{cl,out}}\right) \Big/ \ln\left(\frac{\left(\mathrm{T}_{\mathrm{cd,in}} - \mathrm{T}_{\mathrm{cl,in}}\right)}{\left(\mathrm{T}_{\mathrm{cd,out}} - \mathrm{T}_{\mathrm{cl,out}}\right)}\right) \tag{15}$$

in which G is a function of $\left(\mathrm{T}_{\mathrm{cd,in}}, \mathrm{T}_{\mathrm{cl,in}}, \mathrm{T}_{\mathrm{cd,out}}, \mathrm{T}_{\mathrm{cd,out}}\right)$ that takes into account the type of the heat exchanger [19]. Heat exchanger properties and their symbols are abridged in Tables 7 and 8.

Table 5. Parameters adopted for solution of equations (10-12). The core is added for comparison.

	Symbol	U.P.	L.P.	Downc.	Core	Units
Salt mass	M	475	680	376	1541	kg
Power factor	Q_f	3.89	8.59	2.26	85.26	%

Table 6. Time delay used for pipe modeling in nominal conditions. The original values take into account both the residence time in the 0D components and the transport time in the piping. In the model, the time delay values have been modified according to 0D components time constants.

	Transit Time, s	Model Delay, s	Ref.
Hot leg (Upper Plenum to HE inlet)	7.77	4.7	[4]
Cold leg (HE outlet to Downcomer)	4.9	4.1	[4]
Downcomer to Lower Plenum	3.6	1.3	[4]
Primary HE outlet to Secondary HE inlet	8.24	8.24	[4]
Secondary HE outlet to Primary HE inlet	4.71	4.71	[4]

Table 7. Primary (Salt-Salt) heat exchanger thermal properties, nominal values.

	Symbol	Value	Units	Ref.
Hot fluid mass flow	$\dot{m}_{cd}$	168	kg s^{-1}	[4]
Coolant fluid mass flow	$\dot{m}_{cl}$	105	kg s^{-1}	[4]
Hot fluid heat capacity	cp_{cd}	1983	J kg^{-1} K^{-1}	[9]
Coolant heat capacity	cp_{cl}	2146	J kg^{-1} K^{-1}	[4]
Hot fluid mass in the heat exchanger	M_{cd}	450	kg	[4]*
Coolant mass in the heat exchanger	M_{cl}	170	kg	[4]*
Heat exchange area	A	26	m^2	[20]
Heat exchange coefficient	h	3.7	kW m^{-2} K^{-1}	[20]

* Estimated from other data.

Table 8. Secondary (Salt-Air) heat exchanger thermal properties, nominal values.

	Symbol	Value	Units	Ref.
Hot fluid mass flow	$\dot{m}_{cd}$	105	kg s^{-1}	[4]
Coolant fluid mass flow	$\dot{m}_{cl}$	75	kg s^{-1}	[20]
Hot fluid heat capacity	cp_{cd}	2146	J kg^{-1} K^{-1}	[4]
Coolant heat capacity	cp_{cl}	1011	J kg^{-1} K^{-1}	[20]
Hot fluid mass in the heat exchanger	M_{cd}	616	kg	[20]*
Coolant mass in the heat exchanger	M_{cl}	2.4	kg	[20]*
Heat exchange area	A	65.6	m^2	[20]
Heat exchange coefficient	h	0.24	kW m^{-2} K^{-1}	[20]

* Estimated from other data.

3. SIMULATION RESULTS

The aforementioned modeling approach has been used to reproduce two reactivity driven transients of the MSRE at different power levels [21]. Since frequency domain experimental data are also available, the power-reactivity transfer function has been computed for the full power reactor from the transient result with Samulon's method[3] [22]. In order to reduce the computational complexity, the DNPs have been modeled by means of a single equivalent precursor group for the overall modeling. The effective generated precursor fraction and the decay constant, necessary to equations (7) and (12), are reported in Table 9.
For further insight, the results are also compared with the on-purpose-made, multi-zone transfer function based (0D), ORNL model [23].

3.1 Stationary Results

When studying a MSR, it is common practice to estimate the reactivity loss due to DNP circulation. The results obtained with our 3D channel model in stationary conditions are presented in Table 9, computed by weighting the precursor concentration with equation (9) in the 3D channel. The plena have not been considered for this purpose, thus overestimating the overall reactivity loss. At the nominal fluid velocity, the most circulation-affected DNP groups are the ones with the longest lives, while the shortest life DNP groups decay into the core. The single equivalent precursor group constants are determined from the moving DNP fraction here calculated.

Table 9. DNP data for the U-233 fueled MSRE. The fractions have been divided in the static contributions (S subscript, from ORNL reports) and the moving (M subscript) ones, so that the loss of reactivity due to DNP circulation can be computed.

$\Lambda = 4 \cdot 10^{-4}$ s	g.1	g.2	g.3	g.4	g.5	g.6	Total
λ_i, s^{-1}	0.0126	0.0337	0.139	0.325	1.13	2.5	0.0748*
$\beta_{i\,S}$, *pcm* (ORNL)	22.8	78.8	66.4	73.6	13.60	8.80	264.00
$\beta_{i\,M}$, *pcm* (Present)	7.5	26.4	29.5	46.7	12.21	8.53	130.76
$\Delta\rho_i$, *pcm* (Present)	15.3	52.4	36.9	26.9	1.39	0.27	133.24

*Equivalent value for single DNP group with moving fuel, based on the computed DNP fractions.

3.2 Reactivity Insertion Transient at 8 MW Power Level

The first reproduced transient is the response of the MSRE at 8 MW to a total insertion of 13 pcm, with a rate of 5.3 pcm/s. The high noise in the experimental data is due to the presence of helium bubbles in the core, affecting the salt density [21]. Considering the void coefficients (Table 3), it is sufficient a disturbance of $\pm$0.25% in the overall quantity of void in the core to produce oscillations of $\pm$1.3 pcm, that is compatible with the amplitude of the registered power oscillations.
Nominal plant operation conditions are considered. The simulation time was restricted to the available data points. According to the simulations, the thermal transient of both salt and graphite is not extinguished in such time interval. However, the power has reached the new equilibrium value. The results are presented in Figures 5-7.

[3] The same method was adopted at ORNL together with the classic rod oscillation method for the experimental determination of the transfer function, giving comparable results.

3.3 Reactivity Insertion Transient at 5 MW Power Level

The second reproduced transient is the response of the MSRE at 5 MW to a total insertion of 19 pcm, obtained in two steps with a rate of 5.3 pcm/s. The results are presented in Figures 8-10. The operating conditions in the HEs and the secondary circuit are not known. Therefore, for simulation purpose, the HEs have been set so that the stationary fuel outlet temperature from the primary heat exchanger is equal to the one at 8 MW. Looking at Figure 8, the deviation from experimental data after time 40 s can therefore be explained with the uncertainty on the HEs operating point.

3.4 Analysis of the Results

In general, MSR positive reactivity insertion response can be described as follows: after a first peak due to the reactivity insertion, a plateau is established when the feedback effects re-establish criticality; afterwards, when the fuel re-enters the core at higher temperature, the reactor power decreases and a new plateau is established; then the reactor shows a periodic behavior with these features for some periods, as hinted from the reactor transfer function, that shows a dip both in the module and the phase at the frequency corresponding to the recirculation time and smaller dips at frequencies corresponding to its higher harmonics. Depending on the neutronic characteristics, the build-up of the precursors re-entering the core with the cooled fuel can slightly affect the shape of the second and further plateaus.

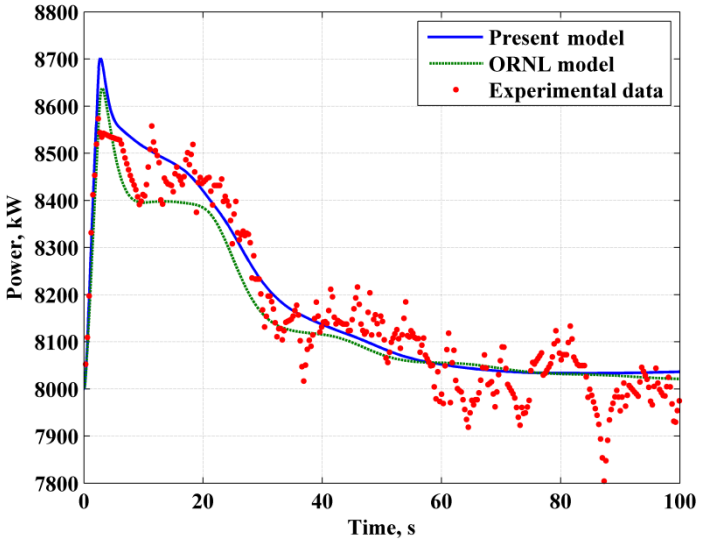

Figure 5. Power response to 13 pcm insertion at 8 MW.

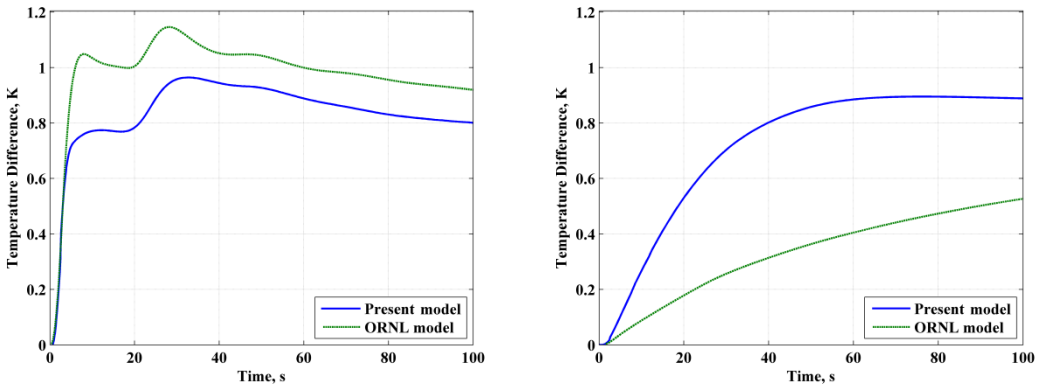

Figure 6. Average Salt (left) and Graphite (right) temperature variation in the core during 13 pcm insertion transient at 8 MW.

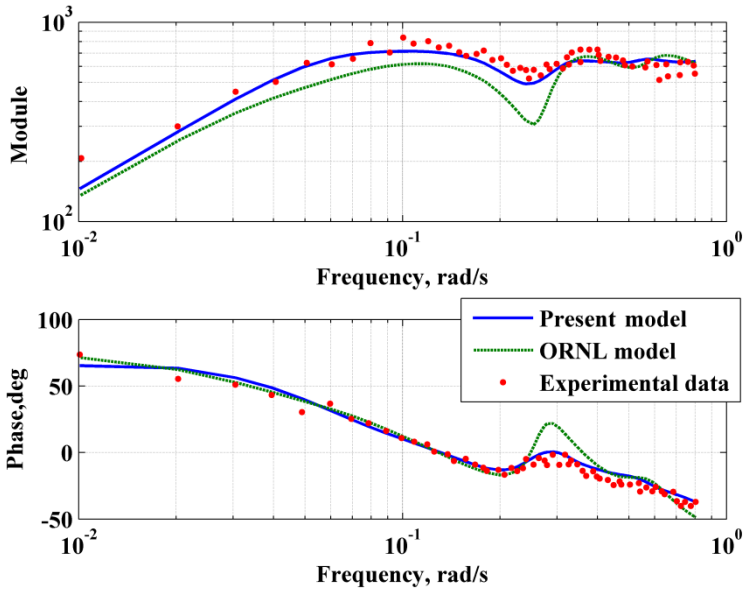

Figure 7. Transfer function of MSRE at 8 MW: module (top) and phase (bottom).

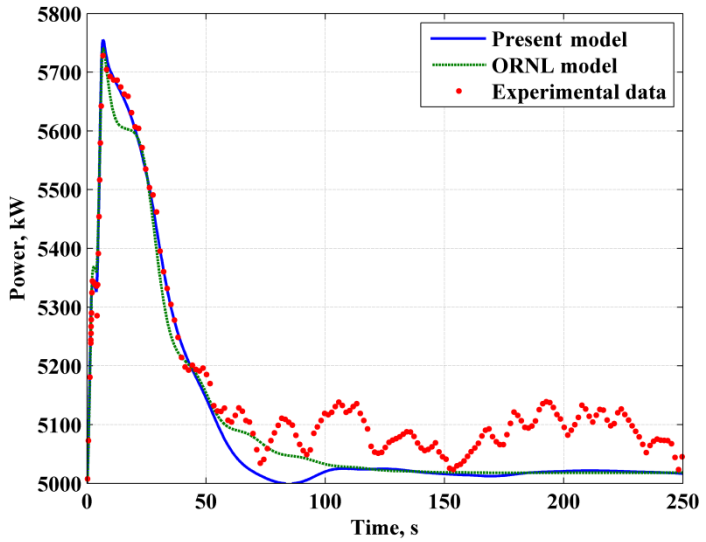

Figure 8. Power response to 19 pcm insertion at 5 MW.

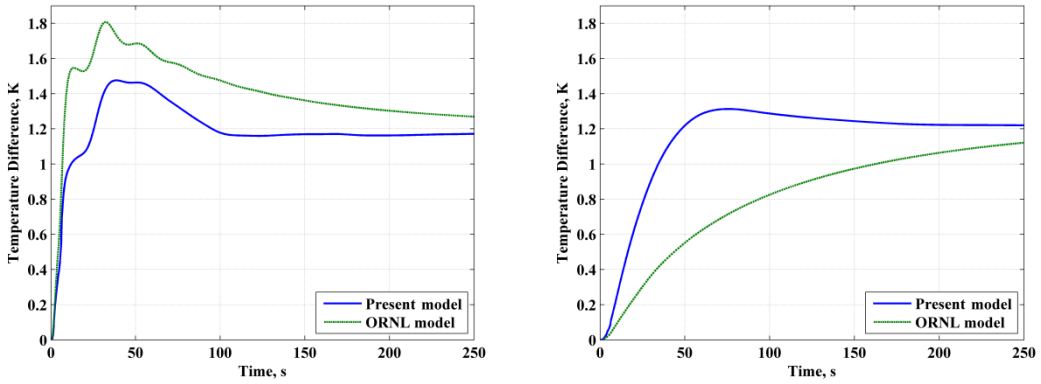

Figure 9. Average Salt (left) and Graphite (right) temperature variation in the core during 19 pcm insertion transient at 5 MW.

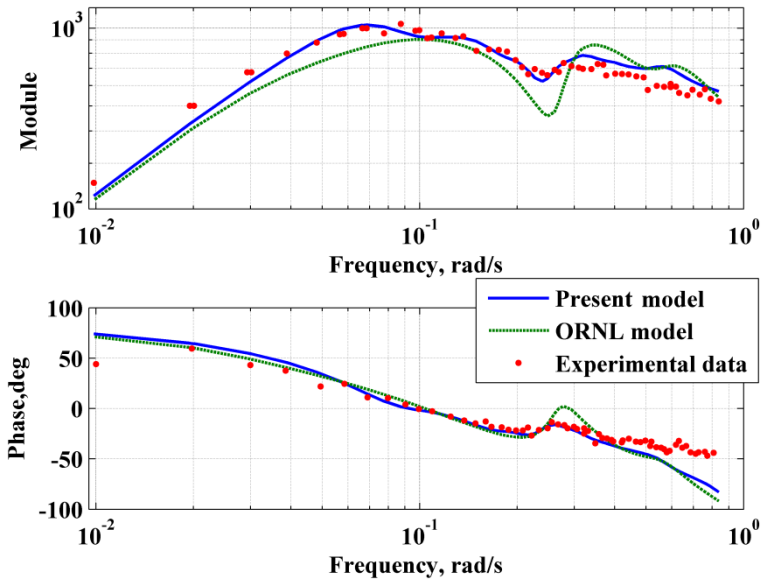

Figure 10. Transfer function of MSRE at 5 MW: module (top) and phase (bottom).

In fact, in the MSRE, the first plateau is not well defined because of the effects of the thermal behavior of the graphite. It was shown by Cammi et al. [24] that graphite, while in stationary conditions is cooled by the fluid fuel, is heated by the fuel during the rise of power, due to the local increase of the salt temperature above the graphite one, with the outcome of an inversion of the heat flux. The possibility of numerically reproducing such phenomenon is related to the spatial solution of the governing equations. On the other hand, when a 0D correlation-based approach is adopted, the energy balance is determined by the fluid and the solid mean temperature (represented by a dotted horizontal red line in Figure 11).

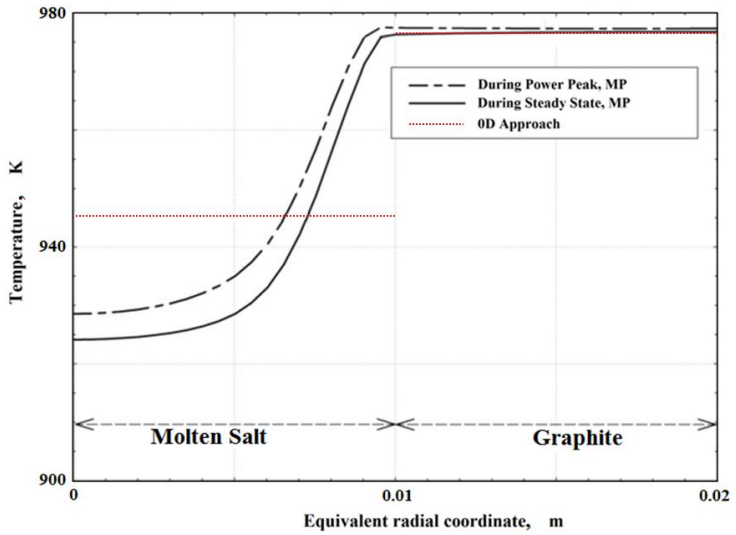

Figure 11. Exemplification of temperature profile in the MSRE channel.

Taking Figure 11 as a reference, it can be inferred that the thermal flux inversion cannot be modeled with this approach, because the average salt temperature does not increase above the graphite one. Considering the dynamic thermal behavior of the two modeling approaches, reported in Figure 6 and 9, it can be noted that the graphite temperature rise is faster in our model than in the ORNL one, because in the former case the graphite is heated, not cooled, by the salt during the power peak. As a consequence, considering the values of the graphite feedback coefficient, the

plateau is not established in our simulation, but it is substituted by a slow decay of the reactor power led by the graphite temperature increase, while the salt temperature is maintained nearly constant.

The frequency domain results are in good agreement with the experimental data. It was observed by Kerlin et al. [25] that the difference in the dip at 0.25 rad/s (Figures 7, 10) between the experimental transfer function and the ORNL model one was due to mixing effects. In the present model, the dynamic mixing effects are taken into account by the 0D plena and downcomer models. However, a further assessment of the plena dynamics - also considering circulation effects on DNP - is needed, possibly adopting a dimensional description, to be added to the multi-scale model.

4. CONCLUSIONS

In this work, a geometric multi-scale modeling approach has been adopted for analyzing the MSRE dynamics. In particular, the reactor core is described by three 3D equivalent channels, modeled and solved with a Finite Elements package, while the remainder of the plant is modeled with a 0D approach. Thus, the DNP and temperature axial distribution in the core and the overall distributions in the single channel can be accurately described. The estimate of the reactivity loss due to the circulation of precursors has been computed from the channel solution.
The reactor power during the transient is determined from a point-kinetics like equation, fed with the data from the 3D channels and the 0D plena. For that purpose, the reactivity coefficients have been computed with the Monte Carlo code Serpent.
The approach has been tested for reactivity driven transient against experimental data for the U-233 fuelled MSRE, both in time and frequency domain. The simulated results and the experimental data are in good agreement. In particular, the adoption of a spatial solution of the energy equation inside a channel allows a better description of the graphite thermal behavior and its consequences at the beginning of the transients. The subdivision of the temperature reactivity effects between the core and the two plena shows the necessity to further investigate the modeling of the peripheral zones of the reactor, both from the neutronic and the thermal-hydraulic point of view.
The MSRE model shows very good agreement with the experimental data thanks to the MP components, and shows a more reliable behavior with respect to previous pure MP models thanks to the loop closure. Overall, the proposed approach seems to be best suited to MSR and traditional reactor that present a channelized geometry. For MSR designs, such as the MSFR [26], which feature a large salt-only volume, the MP modeling should be fully adopted for the core, while the geometric multi-scale approach may be used for the cooling circuits.

ACKNOWLEDGMENTS

We would like to thank Dr. Manule Aufiero (Laboratoire de Physique Subatomique et de Cosmologie, Grenoble, France) for the fruitful discussions and suggestions.

REFERENCES

[1] M. Rosenthal *et al.*, "Molten salt reactors-history, status, and potential", *Nuclear Applications and Technology*, **8(2)**: pp. 107–117 (1970).
[2] K. Furukawa *et al.*, "A road map for the realization of global-scale thorium breeding fuel cycle by single molten-fluoride flow", *Energy Conversion and Management*, **49(7)**, pp. 1832 – 1848. http://dx.doi.org/10.1016/j.enconman.2007.09.027 (2008).
[3] J. Serp *et al.*, "The molten salt reactor (MSR) in generation IV: Overview and perspectives", *Progress in Nuclear Energy*. http://dx.doi.org/10.1016/j.pnucene.2014.02.014 (2014).

[4] R. Robertson, *MSRE design and operations report part I. Description of reactor design*. *Technical Report ORNL-TM-728*, Oak Ridge National Laboratory (1965).
[5] COMSOL, Inc., *COMSOL Multiphysics User's Guide*, version 4.3a edition (2012).
[6] M. Delpech *et al*, "Benchmark of dynamic simulation tools for molten salt reactors. In: *GLOBAL 2003*, pp. 2182–2187, (2003).
[7] J. Leppänen, *Development of a New Monte Carlo Reactor Physics Code*, Ph.D. thesis, Helsinki University of Technology (2007).
[8] R. C. Steffy, *Inherent neutron source in MSRE with clean 233U fuel*. *Technical Report ORNL-TM-2685*, Oak Ridge National Laboratory (1969).
[9] R. E. Thoma, *Chemical aspects of MSRE operations*. *Technical Report ORNL-4658*, Oak Ridge National Laboratory (1971).
[10] G. M. Tolson and A. Taboada, *MSRE control elements: manufacture, inspection, drawings and specification*. *Technical Report ORNL-4123*, Oak Ridge National Laboratory (1967).
[11] D. F. Hoffenbach and C. M. Hopper, *Criticality safety study of the MSRE fuel drain tank cell in building 7503*. *Technical Report ORNL-TM-12642*, Oak Ridge National Laboratory (1994).
[12] P. N. Haubenreich *et al., MSRE design and operations report part III. Nuclear analysis*. *Technical Report ORNL-TM-730*, Oak Ridge National Laboratory (1964).
[13] The Mathworks, Inc., *Simulink User's Guide*, r2012b edition (2012).
[14] M. W. Rosenthal, R. B. Briggs, and P. Kasten, *Molten-Salt Reactor Prorgam semiannual progress report for period ending August 31, 1967*. *Technical Report ORNL-4191*, Oak Ridge National Laboratory (1967).
[15] COMSOL, Inc., *CFD Module User's Guide*, version 4.3a edition (2012).
[16] R. J. Kedl, *Fluid dynamic studies of the Molten-Salt reactor Experiment (MSRE) core*. *Technical Report ORNL-TM-3229*, Oak Ridge National Laboratory (1970).
[17] R. B. Briggs, *Molten-Salt Reactor Prorgam semiannual progress report for period ending July 31, 1964*. *Technical Report ORNL-3708*, Oak Ridge National Laboratory (1964).
[18] G. Bell and S. Glasstone, *Nuclear reactor theory*. Van Nostrand Reinhold Co. (1970).
[19] M. A. Bowman, R.A. and W. Nagle, "Mean temperature difference in design", *Trans. ASME*, **62**, pp. 283– 293 (1940).
[20] C. H. Gabbard, *Reactor power measurement and heat transfer performance in the Molten Salt Reactor Experiment*. *Technical Report ORNL-TM-3002*, Oak Ridge National Laboratory (1970).
[21] R. C. Steffy, *Experiment dynamic analysis of the MSRE with 233U fuel*. *Technical Report ORNL-TM-2997*, Oak Ridge Lational Laboratory (1970).
[22] H. A. Samulon, "Spectrum analysis of transient response curves", *Proceedings of the IRE*, **39(2)**, pp. 175–186. http://dx.doi.org/10.1109/JRPROC.1951.231438 (1951).
[23] R. C. Steffy and P. J. Wood, *Theoretical dynamic analysis of the MSRE with 233U fuel*. *Technical Report ORNL-TM-2571*, Oak Ridge National Laboratory (1969).
[24] A. Cammi *et al.*, "Dimensional effects in the modelling of MSR dynamics: Moving on from simplified schemes of analysis to a multi-physics modelling approach", *Nuclear Engineering and Design*, **246(0)**, pp. 12 – 26. http://dx.doi.org/10.1016/j.nucengdes.2011.08.002 (2011).
[25] T. Kerlin, S. Ball, and R. Steffy, "Theoretical dynamics analysis of the molten-salt reactor experiment", *Nuclear Thechnology*, **10**, pp. 118–132 (1971).
[26] E. Merle-Lucotte, M. Allibert, M. Brovchenko, V. Ghetta, D. Heuer, P. Rubiolo, "Preliminary Design Assessment of the Molten Salt Fast Reactor", *Proceedings of the European Nuclear Conference ENC2012*, Manchester, UK (2012).